Mamba®: Vision Mamba Also Needs Registers

Feng Wang[1]   Jiahao Wang[1]   Sucheng Ren[1]   Guoyizhe Wei[1]   Jieru Mei[1]
Wei Shao[2]   Yuyin Zhou[3]   Alan Yuille[1]   Cihang Xie[3]
[1]Johns Hopkins University   [2] University of Florida   [3]UC Santa Cruz

Abstract

Similar to Vision Transformers, this paper identifies artifacts also present within the feature maps of Vision Mamba. These artifacts, corresponding to high-norm tokens emerging in low-information background areas of images, appear much more severe in Vision Mamba—they exist prevalently even with the tiny-sized model and activate extensively across background regions. To mitigate this issue, we follow the prior solution of introducing register tokens into Vision Mamba. To better cope with Mamba blocks' uni-directional inference paradigm, two key modifications are introduced: 1) evenly inserting registers throughout the input token sequence, and 2) recycling registers for final decision predictions. We term this new architecture Mamba®. Qualitative observations suggest, compared to vanilla Vision Mamba, Mamba®'s feature maps appear cleaner and more focused on semantically meaningful regions. Quantitatively, Mamba® attains stronger performance and scales better. For example, on the ImageNet benchmark, our Mamba®-B attains 83.0% accuracy, significantly outperforming Vim-B's 81.8%; furthermore, we provide the first successful scaling to the large model size with 341M parameters, attaining competitive accuracies of 83.6% and 84.5% for 224×224 and 384×384 inputs, respectively. Additional validation on the downstream semantic segmentation task also supports Mamba®'s efficacy. Code is available at https://github.com/wangf3014/Mamba-Reg.

1. Introduction

Recent advances in State Space Models (SSMs) have showcased their considerable potential in sequence modeling tasks. In contrast to Transformers' quadratic computational complexity with respect to sequence lengths, SSMs operate with linear computational complexity, offering significant efficiency advantages in managing extended sequences. One exemplary instantiation of SSMs is the Mamba architecture [9], which employs selective scan techniques alongside a suite of hardware-optimized designs. This innovation facilitates the efficient training and inference of recurrent models with linear computational complexity and memory overhead. Furthermore, a comprehensive body of recent research [2, 9, 25] substantiates that the Mamba architecture is able to achieve competitive performance levels, on par with Transformers, particularly in processing natural language and audio.

Furthermore, the Mamba architecture has also been successfully extended to a variety of visual tasks [17, 24, 27, 54]. The motivation for this expansion mainly arises from the computational challenges presented by processing high-resolution images and videos. These data types often lead to long input sequences that conventional models struggle to handle effectively or efficiently—*e.g.*, for long-length input, traditional models such as Convolutional Neural Networks (CNNs) suffer from relatively small receptive fields, and Vision Transformers (ViTs) contend with high computational and memory costs. Yet, Vision Mamba (Vim) architectures have shown the potential to mitigate these limitations—recent works demonstrate that they not only manage computational and memory demands more efficiently but also deliver strong performance across a variety of generic visual tasks, including classification, segmentation, and image generation [17, 26, 54].

Despite the competitive benchmark performance, our observations reveal that Mamba's internal modeling exhibits significant issues when processing visual inputs. This issue is similar to the prior observation of ViTs [6], where some outlier tokens located in the less semantic background unexpectedly contain rich global information (showing as high attention scores in the feature map). These unusual feature activations are typically termed artifacts in the existing studies [6]. In this work, we reveal that this artifact issue not only exists but actually is considerably more severe in Vision Mamba. For example, the artifacts are clearly visible in the feature maps of Vim [54], as illustrated in the 2nd and 4th columns of Figure 1, where activations encompass not just semantically significant content, but also extend to expansive yet minimally informative background regions. Furthermore, as quantitatively confirmed in Section 3.2, these artifact tokens are widely present in differ-
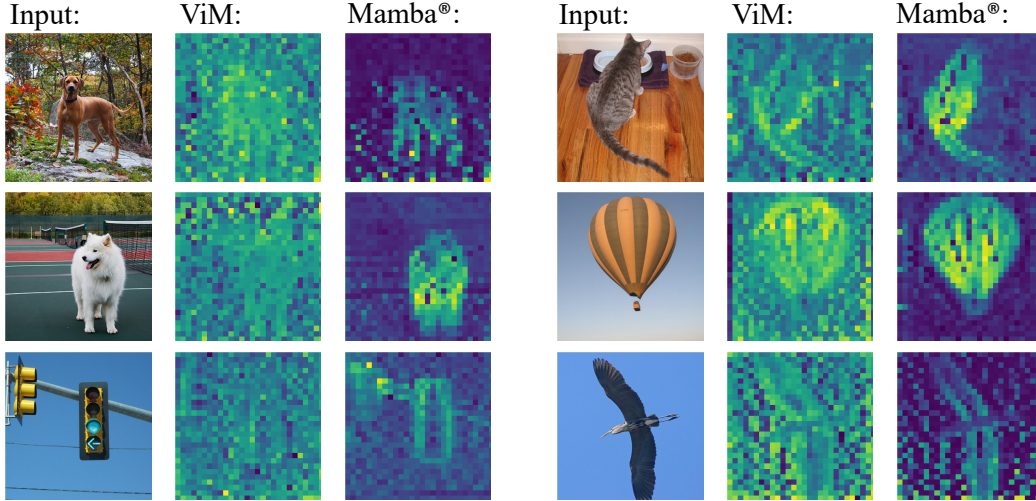
Figure 1. Feature maps of vanilla Vision Mamba (Vim) [54] and our Mamba®. It shows that massive artifacts appear in Vim's feature map, making the model difficult to attend to visually meaningful content within the image. In contrast, our model exhibits much cleaner feature activations, showcasing the significant efficacy of our enhanced architectural design.

ent sizes of Vision Mamba models and possess rich global information. Building upon a previous solution [6], we introduce a straightforward yet effective architectural refinement to Vision Mamba by appending registers—new, input-independent tokens—to the token sequence. Unlike [6] which only appends several register tokens at one end of the input layer, we 1) insert register tokens *evenly* throughout the token sequence; and 2) at the end of the Vision Mamba, concatenate the register tokens to form a comprehensive image representation for the final prediction. We name this enhanced architecture Mamba®.

Empirically, Mamba® showcases advantages on two fronts. Qualitatively, as evidenced by the cleaner feature maps displayed in Figure 1, Mamba® significantly suppresses artifacts, with responses now more focused on visually meaningful content. Meanwhile, as visualized in Figure 6, registers can well capture object-related semantic information for building high-quality image representations. Quantitatively, the improvements in benchmarks are equally compelling. For example, Mamba®-Base achieves an accuracy of 83.0% on ImageNet, notably outperforming the 81.8% accuracy of the vanilla Vim-Base. Furthermore, Mamba® successfully expands the scaling capabilities of Vision Mamba—whereas previous models were limited to configurations no larger than 90M parameters [27, 50, 54], Mamba® can be effectively trained with up to 341M parameters, reaching an impressive 83.6% accuracy on ImageNet; this accuracy can be further boosted to 84.5% by enlarging the image input size to 384×384. For the ADE20k [52] semantic segmentation benchmark, our Mamba® attains a 49.1% evaluation mIoU, which significantly outperforms Vim's best result of 44.9% mIoU [54].

2. Related Work

Generic Visual Backbone Architectures. Modern computer vision predominantly relies on two types of backbone architectures: CNNs that excel in extracting hierarchical features and ViTs that are effective in modeling long-range dependencies. Since the advent of CNNs [23], their structure and scale have undergone a series of significant innovations in recent decades [15, 18, 22, 29, 37, 41]. Unlike CNNs that build spatial dependencies through convolutional operations, ViTs [8] attain a global receptive field by utilizing the self-attention mechanism [44], leading to state-of-the-art performance in a series of downstream visual tasks. Based on this architecture, extensive research has been dedicated to improving its model design [4, 28, 51], enhancing training strategy [42, 43], and advancing self-supervised pretraining and inference frameworks [1, 3, 5, 16, 34, 45, 53].

State Space Models. The concept of State Space Models (SSMs) can be dated back to the 1960s in control systems where it was used to process continuous inputs [20]. With advancements in discretization strategies [10, 13, 32, 40], SSMs have recently been introduced into the field of deep learning, modeling sequential information such as language and speech [11, 12, 38]. Broadly defined, SSMs can refer to any recurrent models with a latent state such as RNNs and the variant architectures such as Linear Attention [21], RetNet [39], and RWKV [33]. More recently, [9] introduced a selective SSM block, namely Mamba, that incorporates structured SSMs with hardware-aware state expansion, leading to a highly efficient recurrent architecture that is competitive to Transformer.
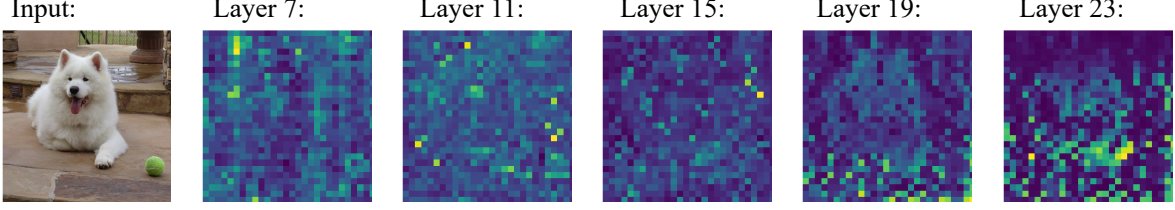
Figure 2. ℓ_2 norm of local image tokens in vision Mamba's different layers. It shows that massive artifacts associated with high-norm tokens appear in the low-information areas, making it hard to distinguish primary objects from the background.
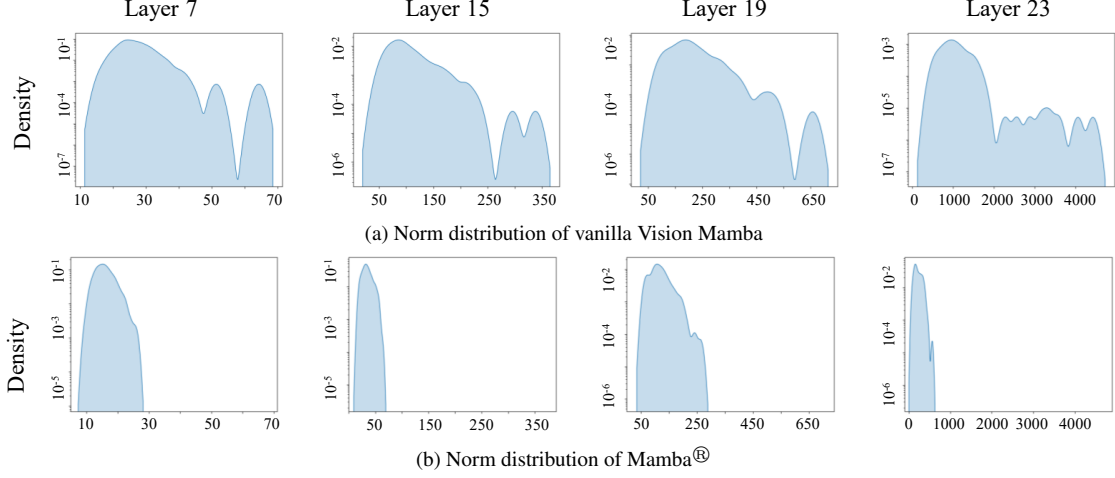

(a) Norm distribution of vanilla Vision Mamba

(b) Norm distribution of Mamba®

Figure 3. Distributions of ℓ_2 normalization values of local outputs across different layers. Compared with the vanilla Vision Mamba model, it quantitatively shows that our Mamba® effectively reduces the number of high-norm outliers.

Mamba Models in Vision. Building upon the Mamba block, a series of follow-up studies have explored the application of SSMs in computer vision. For example, [54] propose a straightforward vision Mamba model by sequentially stacking the Mamba blocks, attaining superior performance than Vision Transformers [8, 42] in both tiny and small model sizes. [27] presents a hierarchical Mamba architecture, showcasing significant results in a series of vision tasks. The study of Mamba-based architectures is continuously explored [14, 24–26, 35, 36, 46–48].

3. Method

3.1. Mamba Preliminaries

The original definition of SSM is a Linear Time-Invariant (LTI) system that projects the input stimulation $x(t) \in \mathbb{R}^L$ to the output response $y(t) \in \mathbb{R}^L$ through a hidden state $h(t) \in \mathbb{C}^N$. For the continuous inputs, the system can be formulated by a group of linear ordinary differential equations as follows:

$$h'(t) = \boldsymbol{A}h(t) + \boldsymbol{B}x(t)$$
$$y(t) = \boldsymbol{C}h(t) + Dx(t), \quad (1)$$

where $\boldsymbol{A} \in \mathbb{R}^{N \times N}$, $\boldsymbol{B} \in \mathbb{R}^N$, $\boldsymbol{C} \in \mathbb{R}^N$, and $D \in \mathbb{R}^1$ denote the weighting parameters.

By discretizing this ordinary differential equation group, the continuous-time SSMs can be integrated to process discrete inputs such as language, speech, and image pixels. To this end, the model can be solved by an analytic solution and then approximated by Zero-Order Hold [9], leading to a discrete model:

$$h_t = \overline{\boldsymbol{A}}h_{t-1} + \overline{\boldsymbol{B}}x_t$$
$$y_t = \boldsymbol{C}h_t + Dx_t, \quad (2)$$

where $\overline{\boldsymbol{A}} = \exp(\Delta A)$, $\overline{\boldsymbol{B}} = (\Delta \boldsymbol{A})^{-1}(\exp(\Delta \boldsymbol{A}) - \boldsymbol{I}) \cdot \Delta \boldsymbol{B}$ are transformed parameters for discrete inputs and Δ is a learnable parameter estimating the discrete interval. Notably, in contrast to the basic recurrent inference, this structured SSM (S4) allows efficient computation by a convolution process with

$$\overline{\boldsymbol{K}} = (\boldsymbol{C}\overline{\boldsymbol{B}}, \boldsymbol{C}\overline{\boldsymbol{A}}\overline{\boldsymbol{B}}, \dots, \boldsymbol{C}\overline{\boldsymbol{A}}^{M-1}\overline{\boldsymbol{B}}) \quad (3)$$

being the kernel and predicting by $\boldsymbol{y} = \boldsymbol{x} * \overline{\boldsymbol{K}}$.

However, the Structural State Space Models' nature of Linear Time-Invariance significantly limits its capacity to
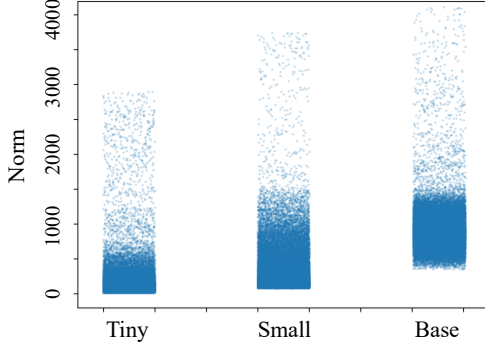
Figure 4. Distributions of ℓ_2 normalization across different sizes of Vision Mamba models. It shows that high-norm outliers widely appear in different sizes of Mamba models.

Table 1. Vim-B's ImageNet accuracy with different features. Using a small portion of high-norm tokens for final prediction attains significantly higher accuracy that that of low-norm tokens.

Feature	Accuracy (%)
class token (default)	81.8
global pooling	81.1
high-norm tokens (top 20%)	81.1
high-norm tokens (top 10%)	81.1
high-norm tokens (top 5%)	81.0
low-norm tokens	79.3

fit contextual information, making it difficult to scale up and achieve performance comparable to Transformers. The Selective State Space Model, also known as Mamba or S6 [9], improves it by introducing input-dependent parameters $\boldsymbol{B} = \boldsymbol{S}_B(x)$, $\boldsymbol{C} = \boldsymbol{S}_C(x)$, and $\Delta = \boldsymbol{S}_\Delta(x)$, leading to a time-varying system that can model more complex inputs. Notably, with associative scan algorithms [31, 38], the Mamba module can be trained and inferred efficiently via parallel computing, with detailed mathematical derivations elaborated in [9].

To adapt Mamba for visual tasks, images are first processed into sequential inputs through patch embedding as in ViT. However, the standard Mamba is a unidirectional model where each token in the sequence can only access information from preceding tokens. This characteristic, while working well with 1-D language signals, significantly constrains the model's capacity to gather contextual information inherently from 2-D visual signals. To overcome this limitation, a common solution is to reconfigure Mamba blocks for bidirectional scanning. Specifically, the sequence is scanned once from start to end and again from end to start, with the outputs from both scans subsequently averaged to obtain a comprehensive representation [54]. We follow this scanning design in all subsequent experiments.

3.2. Feature Artifacts of Vision Mamba

In ViT, an interpretable feature map can be obtained by visualizing the activation scores in their self-attention blocks. Ideally, under appropriate pre-training paradigms, these feature maps are expected to display high attention scores in the informative foreground regions of images and relatively low scores in less semantic background areas. Nevertheless, a considerable amount of outliers often appear in these feature maps, which position-wise correspond to low-information background regions yet exhibit anomalously high attention scores. A recent study [6] has termed these outliers as **feature artifacts**. Specifically, this study reveals that the artifact tokens always possess high normalization values and, during inference, they tend to discard their local information in favor of retaining global features, thereby "compromising" the quality of the feature map.

This work identifies a similar issue in Vision Mamba models. First, by computing the ℓ_2 distances between vanilla Vision Mamba's global and local outputs, we observe a considerable amount of activations in background areas (shown in Figure 1). Further analysis of their normalization reveals that these background activations also exhibit high normalization values, akin to the artifacts observed in ViTs. For example, by visualizing the ℓ_2 normalization of vanilla Vision Mamba's local outputs in Figure 2, we can observe a significant presence of high-norm tokens in the background, even blurring the distinction between foreground and background regions. Quantitatively, we plot the norm distributions of vanilla Vision Mamba in Figure 3a, where it clearly displays a number of outliers with high normalization, confirming consistency with previous findings in ViTs as discussed in [6].

Furthermore, it is equally noteworthy that these artifacts in Vision Mamba function similarly to those in ViTs in retaining global representations [6]. As reported in Table 1, the vanilla Vision Mamba model can obtain 81.0% ImageNet accuracy by merely using the average of top 5% high norm tokens as a global feature, which is only 0.1% lower than that of pooling all local tokens. Increasing this threshold to top 10% or 20% high norm tokens further enables the model to match the accuracy of using global pooling. In contrast, relying on the remaining 80% of relatively low-norm tokens results in a performance drop to 79.3%.

Yet differently, we observe that the artifact issues are considerably more severe in Vision Mamba than in ViTs: these artifacts appear more prevalent in the background areas and exhibit higher normalization values than those observed in ViTs. As shown in Figure 3a, the average norm of the outlier tokens increases rapidly with the depth of layers, reaching over 4000 by the 23rd layer. Compared to the norms below 100 in shallower features, these extremely high-norm artifacts can easily affect feature extraction and pose significant challenges to model optimization, which may poten-
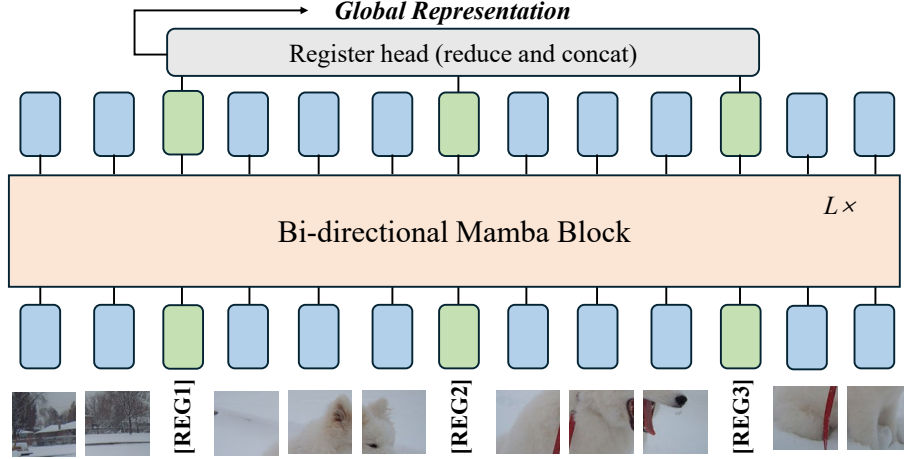
Figure 5. Framework of Mamba$^®$. We address Vision Mamba's artifact issues by evenly inserting input-independent register tokens into the input sequence. In the final layer, we concatenate the output of register tokens to form a global representation for final predictions.

tially explain the instability issues and scaling difficulties encountered in Vision Mamba. Additionally, unlike ViTs where artifacts predominantly appear in larger models, they are present even in the tiny Vision Mamba models and intensify with increasing model size, as illustrated in Figure 4. These observations altogether suggest that the artifact issues are crucial for Vision Mamba models and need to be urgently addressed.

3.3. Mamba$^®$: Vision Mamba with Registers

Following the solution of removing artifacts in ViT [6], we propose to address this issue by introducing register tokens into Vision Mamba. We term our new architecture Mamba$^®$. Unlike the previous method [6] which only appends register tokens at one end of the input sequence, we hypothesize that by distributing the register tokens more densely throughout the sequence, our method can 1) better address the more pervasive artifact issue that is unique to vision mamba; and 2) helps capture global representation that is often missed in vision mamba due to its unidirectional nature. The framework of Mamba$^®$ is illustrated in Figure 5. Overall, we follow the backbone architecture of vanilla Vision Mamba (Vim) [54], where the input image is first decomposed into a sequence of non-overlapping patches and then fed into a stack of bi-directional Mamba blocks. Based on this plain architecture, we make the following two simple yet very effective modifications to build our Mamba$^®$.

Sparsely distributed register tokens. The input sequence of Mamba$^®$is composed of m image tokens produced by patch embedding and n register tokens evenly inserted between them. Contrary to the self-attention module where token outputs are agnostic to their positions, in Mamba, it is crucial to strategically place the registers to ensure effective interaction with local tokens. Intuitively, for the recurrent Mamba model, sparsely distributed registers facilitate capturing and preserving important semantic information across different positions. In our experiments, we also empirically confirm that this token positioning enhances both quantitative and qualitative performance.

Register head for final prediction. Different from ViTs which simply discard registers during the final prediction, we observe that recycling them as a global representation yields significant improvements for vision Mamba. Specifically, given n d-dimensional register vectors, we first apply a linear layer to reduce their dimensionality by a factor of r, and then concatenate them into a single vector in dimension of $n \times d/r$, which we refer to as the register head. Note that the choice to concatenate, rather than average, is motivated by the multi-head mechanism in self-attention, where concatenation is more effective at retaining information from all heads. The detailed configurations of Mamba$^®$can be found in Table 2.

In addition, as shown in Figure 6, we observe that in certain cases, our registers can interestingly display distinct feature patterns highlighting different objects or semantic elements within a scene, an intriguing aspect that is not explicitly optimized. Given that Mamba currently lacks a multi-head mechanism, this property could have the potential to offer a valuable dimension for interpreting Mamba's feature representations.

4. Experiments

4.1. Experimental Settings

We primarily evaluate our Mamba$^®$ on the standard ImageNet [7] dataset, which consists of ∼1.28 million training images and 50,000 validation images spread across 1,000

Table 2. Configurations of Mamba®series models. We set patch size to 16 by default for all models.

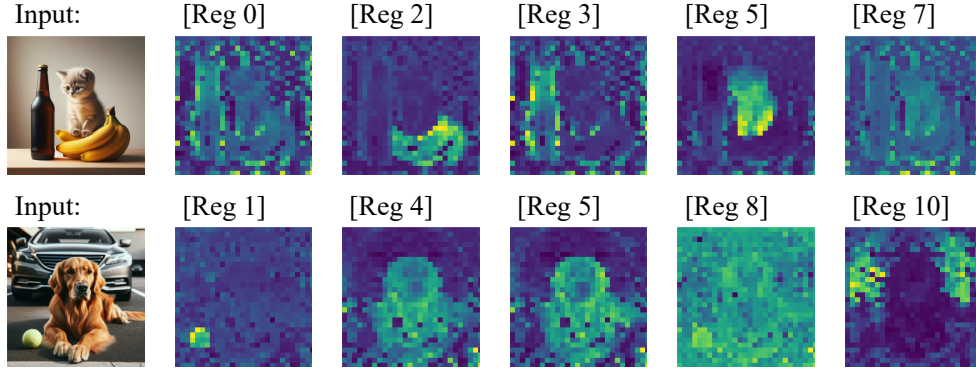| Model	Depth	Embed dim (d)	#Registers (n)	Reduce (r)	#Params
Mamba®-Tiny	24	192	12	1	9M
Mamba®-Small	24	384	12	2	28M
Mamba®-Base	24	768	12	4	98M
Mamba®-Large	48	1024	16	8	341M

Figure 6. Feature maps for different register tokens. The registers sometimes can attend to different parts or semantics with an image. Similar to the multi-head self-attention mechanism, this property is not required but naturally emerges from training.

categories. Our training setup mostly follows the protocols established in DeiT [42]. Specifically, we use AdamW optimizer [30] with a momentum of 0.9, a weight decay of 0.05, a cosine annealing learning rate starting at 1×10^{-3}, a batch size of 1024 for Mamba®-Tiny, Small, and Base, and a batch size of 2048 for Mamba®-Large. For better efficiency and preventing over-fitting, we train each model for 300 epochs in 128×128 input size and fine-tune in 224×224 with stronger data augmentation strategies. We also empirically find a 100-epoch intermediate finetuning with weak augmentation can further improve the results. In total, the training process leads to ∼230 effective training epochs in 224×224 image size, yet significantly outperforms its 300-epoch counterparts. A detailed training recipe can be found in the Appendix.

We further evaluate models' downstream performance on semantic segmentation using the ADE20k [52] dataset, which comprises 150 fine-grained semantic categories distributed across 20K training images, 2K validation images, and 3K test images. Following the existing baseline models [42, 54], we choose UperNet [49] as the segmentation head. We utilize AdamW optimizer with a weight decay of 0.01. The models are optimized with a total batch size of 16 for 160k iterations.

4.2. Main Results

Image classification. As illustrated in Table 3, our Mamba® demonstrates strong performance on the ImageNet-1k classification benchmark. Compared to the existing pure Mamba architecture, Vim [54], Mamba® shows a significant improvement, outperforming Vim by 1.3% for the Tiny model and by 0.6% for the Small model. More importantly, compared to Vim, our Mamba® exhibits significant enhancement in scalability: we successfully train a Base (99M parameters, achieving 83.0% accuracy) and even a Large (341M parameters, achieving 83.2% accuracy) size Mamba architectures in vision, demonstrating that Mamba-based causal models can also learn with hundreds of million parameters in image modeling. This performance can be further enhanced by finetuning with the input resolutions increased to 384 × 384—our highest accuracy is 84.5%, which outperforms all prior Mamba variants in ImageNet classification.

Semantic segmentation. As shown in Table 5, Mamba® consistently exhibits superior semantic segmentation performance on the ADE20k dataset [52]. For example, when compared with Vim-S [54], our Mamba®-S achieves an improvement of 0.4% mIoU. By further scaling up, our Mamba®-B model (featuring 132M parameters) records an mIoU of 47.7%, notably outperforming a similarly-sized DeiT-B model by 2.2% mIoU (results for DeiT are referenced from [27]). Additionally, our Mamba®-L (with 377M parameters) also shows great scalability in the segmentation task, achieving 49.1% mIoU on the ADE20k benchmark.

Table 3. ImageNet classification results. The throughput is tested on an A100 GPU during training. The memory overhead is measured with a batch size of 128 on a single GPU. Our results are highlighted in `blue`.

Model	Image size	Eff. epochs	Parameters	Throughput	Memory	Accuracy (%)
Convolutional networks:						
ResNet-50 [15]	224^2	300	25M	2388	6.6G	76.2
ResNet-152 [15]	224^2	300	60M	1169	12.5G	78.3
EfficientNet-B3 [41]	300^2	300	12M	546	19.7G	81.6
EfficientNet-B5 [41]	456^2	300	30M	143	78.5G	83.6
EfficientNet-B7 [41]	560^2	300	66M	61	>80G	84.3
ConvNeXt-T [29]	224^2	300	29M	635	8.3G	82.1
ConvNeXt-S [29]	224^2	300	50M	412	13.1G	83.1
ConvNeXt-B [29]	224^2	300	89M	305	17.9G	83.8
Vision Transformers:						
ViT-B/16 [8]	384^2	300	86M	201	63.8G	77.9
ViT-L/16 [8]	384^2	300	307M	95	>80G	76.5
DeiT-S [42]	224^2	300	22M	1924	6.8G	79.8
DeiT-B [42]	224^2	300	86M	861	14.4G	81.8
DeiT-B [42]	384^2	300	86M	201	63.8G	83.1
DeiT-III-B [43]	224^2	315	86M	861	14.4G	83.2
Hybrid architecture (2D convolution + Mamba):						
VMamba-T [27]	224^2	300	31M	464	7.6G	82.5
VMamba-S [27]	224^2	300	50M	313	27.6G	83.6
VMamba-B [27]	224^2	300	89M	246	37.1G	83.9
LocalVMamba-S [19]	224^2	300	50M	289	28.0G	83.7
PlainMamba-L3 [50]	224^2	300	50M	256	28.5G	82.3
Pure Mamba architecture:						
Vim-T [54]	224^2	300	7M	750	4.8G	76.1
Vim-S [54]	224^2	300	26M	395	9.4G	80.5
LocalVim-S [19]	224^2	300	28M	404	9.6G	81.2
Mamba®-T	224^2	300	9M	746	5.1G	77.4
Mamba®-S	224^2	230	28M	391	9.9G	81.4
Mamba®-B	224^2	230	99M	196	20.3G	83.0
	384^2	230	99M	63	51.4G	**84.3**
Mamba®-L	224^2	230	341M	67	55.5G	83.6
	384^2	230	342M	23	>80G	**84.5**

4.3. Ablation Study

Basically, in our models, introducing register tokens brings two effects: 1) the inherent benefits of the register itself, including the reduced number of high-norm artifact tokens (see Figure 3b) and enhanced feature extraction capabilities; and 2) the changes in output dimensions caused by the register head (i.e., the $n \times d/r$ output dimension). Here we present ablation studies to separately demonstrate the impact of these two effects on predictive performance.

Number of registers. We first ablate how the number of registers affects the model's ImageNet accuracy. As summarized in Table 6, inserting registers generally leads to consistent performance enhancements, with 0.8% and 1.0% higher accuracy compared with vanilla Mamba architectures in both the Small size and the Base size. Additionally, we observe that simply increasing the output dimension has little benefit to the performance. For example, by projecting Vim-Base's 768-dimensional latent output size into 2304, the accuracy is only improved by 0.1%. Furthermore, we observed that using 12 registers is a sweet point for both the Small size and the Base size; after that, the performance will saturate and may even drop if the final aggregated feature dimension is high (e.g., 4608).

Registers design choice. Next, we ablate our design choices of registers, i.e., evenly inserting registers and reuse them for final prediction. The results are reported in Table 4. First, we note the performance is sensitive to the positioning

Table 4. Ablation study of register positions and final prediction protocols. R and I denote register and image tokens respectively. The column "Final prediction" implies how global feature is computed. R_1 *only:* use one of the registers and discard others. *"Reduce and concat"* is our default setting that leverages a linear layer to reduce registers' dimension and concatenate them as global representation.

Mode	Register positions	Final prediction	Accuracy (%)
Head	R_1 R_2 I_1 I_2 I_3 I_4 I_5 I_6	R_1 only	81.3
		Mean of registers	81.4
		Reduce and concat	82.1
Middle	I_1 I_2 I_3 R_1 R_2 I_4 I_5 I_6	R_1 only	81.8
		Mean of registers	82.0
		Reduce and concat	82.6
Even	I_1 I_2 R_1 I_3 I_4 R_2 I_5 I_6	R_1 only	81.7
		Mean of registers	82.2
		Reduce and concat	**83.0**

Table 5. Semantic segmentation results on ADE20K. All models are trained with an UperNet head and 512×512 input size.

Backbone	#Parameters	mIoU (%)
ResNet-50	67M	41.2
ResNet-101	86M	44.9
DeiT-S	58M	43.8
DeiT-B	144M	45.5
Vim-Ti	13M	41.0
Vim-S	46M	44.9
Mamba$^{\circledR}$-S	56M	45.3
Mamba$^{\circledR}$-B	132M	47.7
Mamba$^{\circledR}$-L	377M	**49.1**

Table 6. Ablation study of registers with a Mamba$^{\circledR}$-Base (d=768). The final output dimension is calculated by $d \times n/r$, where $r < 1$ denotes increasing the dimension. Note that the case $n = r = 1$ is equivalent to vanilla Vision Mamba (Vim) with a class token (marked in gray. Our default setup is highlighted in blue. The best result is **bolded**.

#Reg (n)	Rdc (r)	Final dim.	Acc. (%)
1	1	768	81.8
1	1/3	2304	82.0
3	1	2304	82.8
6	2	2304	82.8
12	4	2304	**83.0**
24	4	4608	82.6

of the registers. For instance, positioning all registers at the beginning of the sequence results in a performance decrease of 0.8% (82.1% vs. 83.0%). Similarly, positioning all registers in the middle of the sequence, the best strategy reported by Vim [54], still led to a 0.3% drop in performance, which suggests that the sparse distribution of registers helps with feature extraction for Vision Mamba. These noticeable performance gaps highlight the necessity of evenly inserting registers between image tokens, as the recurrent formulation makes Mamba sensitive to positions in the sequence.

Further distinctions in register utility are observed when comparing with previous findings [6], which indicate that registers primarily aid in enhancing ViT's feature representation. In contrast, our study demonstrates that the registers play a crucial role in boosting the quantitative performance of Vision Mamba architectures. Notably, utilizing our default method of evenly distributed registers and reusing all for the final prediction achieved an accuracy of 83.0%, surpassing the approach that uses only one register (R_1 only;

the rest of the tokens are discarded) by 1.2%. These results affirm that registers constitute a vital component of the Vision Mamba architecture.

5. Conclusion

In this paper, we explored the nature of artifacts within the feature maps of Vision Mamba, contrasting these with those observed in Vision Transformers. Specifically, we implemented a novel architecture named Mamba$^{\circledR}$, incorporating registers strategically to enhance image processing. Our empirical assessments demonstrate that, qualitatively, Mamba$^{\circledR}$ not only reduces the presence of artifacts but also sharpens the focus on semantically relevant areas within images, leading to cleaner and more effective feature maps. Quantitatively, Mamba$^{\circledR}$ not only surpasses its predecessors in accuracy but also exhibits superior scalability, handling larger model sizes with competitive accuracy. We hope this work can establish a solid backbone for future research in optimizing Mamba architectures in vision.

Acknowledgment

References

[1] Hangbo Bao, Li Dong, and Furu Wei. BEiT: BERT pretraining of image transformers. In *ICLR*, 2022. 2

[2] Ali Behrouz, Michele Santacatterina, and Ramin Zabih. Mambamixer: Efficient selective state space models with dual token and channel selection. *arXiv preprint arXiv:2403.19888*, 2024. 1

[3] Mathilde Caron, Hugo Touvron, Ishan Misra, Hervé Jégou, Julien Mairal, Piotr Bojanowski, and Armand Joulin. Emerging properties in self-supervised vision transformers. In *ICCV*, 2021. 2

[4] Chun-Fu Richard Chen, Quanfu Fan, and Rameswar Panda. Crossvit: Cross-attention multi-scale vision transformer for image classification. In *ICCV*, 2021. 2

[5] Xinlei Chen, Saining Xie, and Kaiming He. An empirical study of training self-supervised vision transformers. In *ICCV*, 2021. 2

[6] Timothée Darcet, Maxime Oquab, Julien Mairal, and Piotr Bojanowski. Vision transformers need registers. In *ICLR*, 2024. 1, 2, 4, 5, 8

[7] Jia Deng, Wei Dong, Richard Socher, Li-Jia Li, Kai Li, and Li Fei-Fei. ImageNet: A large-scale hierarchical image database. In *CVPR*, 2009. 5

[8] Alexey Dosovitskiy, Lucas Beyer, Alexander Kolesnikov, Dirk Weissenborn, Xiaohua Zhai, Thomas Unterthiner, Mostafa Dehghani, Matthias Minderer, Georg Heigold, Sylvain Gelly, Jakob Uszkoreit, and Neil Houlsby. An image is worth 16x16 words: Transformers for image recognition at scale. In *ICLR*, 2021. 2, 3, 7

[9] Albert Gu and Tri Dao. Mamba: Linear-time sequence modeling with selective state spaces. *arXiv preprint arXiv:2312.00752*, 2023. 1, 2, 3, 4

[10] Albert Gu, Tri Dao, Stefano Ermon, Atri Rudra, and Christopher Ré. Hippo: Recurrent memory with optimal polynomial projections. In *NeurIPS*, 2020. 2

[11] Albert Gu, Isys Johnson, Karan Goel, Khaled Saab, Tri Dao, Atri Rudra, and Christopher Ré. Combining recurrent, convolutional, and continuous-time models with linear state space layers. In *NeurIPS*, 2021. 2

[12] Albert Gu, Karan Goel, and Christopher Ré. Efficiently modeling long sequences with structured state spaces. In *ICLR*, 2022. 2

[13] Albert Gu, Isys Johnson, Aman Timalsina, Atri Rudra, and Christopher Ré. How to train your hippo: State space models with generalized orthogonal basis projections. In *ICLR*, 2023. 2

[14] Ali Hatamizadeh and Jan Kautz. Mambavision: A hybrid mamba-transformer vision backbone. *arXiv preprint arXiv:2407.08083*, 2024. 3

[15] Kaiming He, Xiangyu Zhang, Shaoqing Ren, and Jian Sun. Deep residual learning for image recognition. In *CVPR*, 2016. 2, 7

[16] Kaiming He, Xinlei Chen, Saining Xie, Yanghao Li, Piotr Dollár, and Ross Girshick. Masked autoencoders are scalable vision learners. In *CVPR*, 2022. 2

[17] Vincent Tao Hu, Stefan Andreas Baumann, Ming Gui, Olga Grebenkova, Pingchuan Ma, Johannes Fischer, and Bjorn Ommer. Zigma: Zigzag mamba diffusion model. *arXiv preprint arXiv:2403.13802*, 2024. 1

[18] Gao Huang, Zhuang Liu, Laurens Van Der Maaten, and Kilian Q Weinberger. Densely connected convolutional networks. In *CVPR*, 2017. 2

[19] Tao Huang, Xiaohuan Pei, Shan You, Fei Wang, Chen Qian, and Chang Xu. Localmamba: Visual state space model with windowed selective scan. *arXiv preprint arXiv:2403.09338*, 2024. 7

[20] Rudolph Emil Kalman. A new approach to linear filtering and prediction problems. 1960. 2

[21] Angelos Katharopoulos, Apoorv Vyas, Nikolaos Pappas, and François Fleuret. Transformers are rnns: Fast autoregressive transformers with linear attention. In *ICML*, 2020. 2

[22] Alex Krizhevsky, Ilya Sutskever, and Geoffrey E Hinton. Imagenet classification with deep convolutional neural networks. In *NeurIPS*, 2012. 2

[23] Yann LeCun, Léon Bottou, Yoshua Bengio, and Patrick Haffner. Gradient-based learning applied to document recognition. *Proceedings of the IEEE*, 1998. 2

[24] Kunchang Li, Xinhao Li, Yi Wang, Yinan He, Yali Wang, Limin Wang, and Yu Qiao. Videomamba: State space model for efficient video understanding. *arXiv preprint arXiv:2403.06977*, 2024. 1, 3

[25] Opher Lieber, Barak Lenz, Hofit Bata, Gal Cohen, Jhonathan Osin, Itay Dalmedigos, Erez Safahi, Shaked Meirom, Yonatan Belinkov, Shai Shalev-Shwartz, et al. Jamba: A hybrid transformer-mamba language model. *arXiv preprint arXiv:2403.19887*, 2024. 1

[26] Jiarun Liu, Hao Yang, Hong-Yu Zhou, Yan Xi, Lequan Yu, Yizhou Yu, Yong Liang, Guangming Shi, Shaoting Zhang, Hairong Zheng, et al. Swin-umamba: Mamba-based unet with imagenet-based pretraining. *arXiv preprint arXiv:2402.03302*, 2024. 1, 3

[27] Yue Liu, Yunjie Tian, Yuzhong Zhao, Hongtian Yu, Lingxi Xie, Yaowei Wang, Qixiang Ye, and Yunfan Liu. Vmamba: Visual state space model. *arXiv preprint arXiv:2401.10166*, 2024. 1, 2, 3, 6, 7

[28] Ze Liu, Yutong Lin, Yue Cao, Han Hu, Yixuan Wei, Zheng Zhang, Stephen Lin, and Baining Guo. Swin transformer: Hierarchical vision transformer using shifted windows. In *ICCV*, 2021. 2

[29] Zhuang Liu, Hanzi Mao, Chao-Yuan Wu, Christoph Feichtenhofer, Trevor Darrell, and Saining Xie. A convnet for the 2020s. In *CVPR*, 2022. 2, 7

[30] Ilya Loshchilov and Frank Hutter. Decoupled weight decay regularization. In *ICLR*, 2019. 6

[31] Eric Martin and Chris Cundy. Parallelizing linear recurrent neural nets over sequence length. In *ICLR*, 2018. 4

[32] Eric Nguyen, Karan Goel, Albert Gu, Gordon Downs, Preey Shah, Tri Dao, Stephen Baccus, and Christopher Ré. S4nd: Modeling images and videos as multidimensional signals with state spaces. In *NeurIPS*, 2022. 2

[33] Bo Peng, Eric Alcaide, Quentin Anthony, Alon Albalak, Samuel Arcadinho, Huanqi Cao, Xin Cheng, Michael Chung, Matteo Grella, Kranthi Kiran GV, et al. Rwkv: Reinventing rnns for the transformer era. *arXiv preprint arXiv:2305.13048*, 2023. 2

[34] Alec Radford, Jong Wook Kim, Chris Hallacy, Aditya Ramesh, Gabriel Goh, Sandhini Agarwal, Girish Sastry, Amanda Askell, Pamela Mishkin, Jack Clark, et al. Learning transferable visual models from natural language supervision. In *ICML*, 2021. 2

[35] Sucheng Ren, Xianhang Li, Haoqin Tu, Feng Wang, Fangxun Shu, Lei Zhang, Jieru Mei, Linjie Yang, Peng Wang, Heng Wang, et al. Autoregressive pretraining with mamba in vision. *arXiv preprint arXiv:2406.07537*, 2024. 3

[36] Sucheng Ren, Yaodong Yu, Nataniel Ruiz, Feng Wang, Alan Yuille, and Cihang Xie. M-var: Decoupled scale-wise autoregressive modeling for high-quality image generation. *arXiv preprint arXiv:2411.10433*, 2024. 3

[37] Karen Simonyan and Andrew Zisserman. Very deep convolutional networks for large-scale image recognition. In *ICLR*, 2015. 2

[38] Jimmy TH Smith, Andrew Warrington, and Scott W Linderman. Simplified state space layers for sequence modeling. In *ICLR*, 2022. 2, 4

[39] Yutao Sun, Li Dong, Shaohan Huang, Shuming Ma, Yuqing Xia, Jilong Xue, Jianyong Wang, and Furu Wei. Retentive network: A successor to transformer for large language models. *arXiv preprint arXiv:2307.08621*, 2023. 2

[40] Corentin Tallec and Yann Ollivier. Can recurrent neural networks warp time? In *ICLR*, 2018. 2

[41] Mingxing Tan and Quoc Le. Efficientnet: Rethinking model scaling for convolutional neural networks. In *ICML*, 2019. 2, 7

[42] Hugo Touvron, Matthieu Cord, Matthijs Douze, Francisco Massa, Alexandre Sablayrolles, and Hervé Jégou. Training data-efficient image transformers & distillation through attention. In *ICML*, 2021. 2, 3, 6, 7, 11

[43] Hugo Touvron, Matthieu Cord, and Hervé Jégou. Deit iii: Revenge of the vit. In *ECCV*, 2022. 2, 7, 11

[44] Ashish Vaswani, Noam Shazeer, Niki Parmar, Jakob Uszkoreit, Llion Jones, Aidan N Gomez, Łukasz Kaiser, and Illia Polosukhin. Attention is all you need. In *NeurIPS*, 2017. 2

[45] Feng Wang, Jieru Mei, and Alan Yuille. Sclip: Rethinking self-attention for dense vision-language inference. In *ECCV*, 2024. 2

[46] Feng Wang, Timing Yang, Yaodong Yu, Sucheng Ren, Guoyizhe Wei, Angtian Wang, Wei Shao, Yuyin Zhou, Alan Yuille, and Cihang Xie. Causal image modeling for efficient visual understanding. *arXiv preprint arXiv:2410.07599*, 2024. 3

[47] Feng Wang, Yaodong Yu, Guoyizhe Wei, Wei Shao, Yuyin Zhou, Alan Yuille, and Cihang Xie. Scaling laws in patchification: An image is worth 50,176 tokens and more. *arXiv preprint arXiv:2502.03738*, 2025.

[48] Guoyizhe Wei and Rama Chellappa. Vit-linearizer: Distilling quadratic knowledge into linear-time vision models. *arXiv preprint arXiv:2504.00037*, 2025. 3

[49] Tete Xiao, Yingcheng Liu, Bolei Zhou, Yuning Jiang, and Jian Sun. Unified perceptual parsing for scene understanding. In *ECCV*, 2018. 6

[50] Chenhongyi Yang, Zehui Chen, Miguel Espinosa, Linus Ericsson, Zhenyu Wang, Jiaming Liu, and Elliot J Crowley. Plainmamba: Improving non-hierarchical mamba in visual recognition. *arXiv preprint arXiv:2403.17695*, 2024. 2, 7

[51] Li Yuan, Yunpeng Chen, Tao Wang, Weihao Yu, Yujun Shi, Zi-Hang Jiang, Francis EH Tay, Jiashi Feng, and Shuicheng Yan. Tokens-to-token vit: Training vision transformers from scratch on imagenet. In *ICCV*, 2021. 2

[52] Bolei Zhou, Hang Zhao, Xavier Puig, Tete Xiao, Sanja Fidler, Adela Barriuso, and Antonio Torralba. Semantic understanding of scenes through the ade20k dataset. *IJCV*, 2019. 2, 6

[53] Chong Zhou, Chen Change Loy, and Bo Dai. Extract free dense labels from clip. In *ECCV*, 2022. 2

[54] Lianghui Zhu, Bencheng Liao, Qian Zhang, Xinlong Wang, Wenyu Liu, and Xinggang Wang. Vision mamba: Efficient visual representation learning with bidirectional state space model. In *ICML*, 2024. 1, 2, 3, 4, 5, 6, 7, 8

Appendix A: Technical Details

Table 7. Pre-training configurations

Configuration	Small	Base	Large
input size		128	
epochs		300	
optimizer		AdamW	
weight decay		0.05	
base learning rate	5e-4	2e-4	2e-4
batch size	1024	2048	2048
drop path		0.1	
label smoothing		✗	
random erasing		✗	
Rand Augmentation		✗	
repeated augmentation		✓	
ThreeAugmentation		✓	

Table 8. Intermediate training configurations

Configuration	Small	Base	Large
input size		224	
epochs		100	
optimizer		AdamW	
weight decay		0.05	
base learning rate		2e-4	
batch size		1024	
drop path	0.2	0.4	0.4
label smoothing		✗	
random erasing		✗	
Rand Augmentation		✗	
repeated augmentation		✓	
ThreeAugmentation		✓	

Table 9. Fine-tuning configurations

Configuration	Small	Base	Large
input size		224	
epochs		20	
optimizer		AdamW	
weight decay		0.1	
base learning rate		1e-5	
batch size		512	
drop path	0.2	0.4	0.6
label smoothing		0.1	
random erasing		✗	
Rand Augmentation		rand-m9-mstd0.5-inc1	
repeated augmentation		✗	
ThreeAugmentation		✗	

We train Mamba®-Tiny by the configurations of DeiT-Tiny [42] but follow a weaker data augmentation strategy used in [43]. For bigger sizes of Mamba®models, we use a three-stage training approach to prevent over-fitting and reduce effective training epochs. We summarize the recipes of pre-training, intermediate training, and fine-tuning in Table 7, Table 8, and Table 9, respectively. For all stages, the learning rate is calculated by base lr × batch size / 512, following a cosine decay scheduling with 5 epochs warmup. We use color jitter with a factor of 0.3, mixup and cutmix with alpha setting to 0.8 and 1.0, respectively.

Appendix B: Theoretical Justification

We demonstrate that Mamba® performs well because it effectively addresses the ***vanishing gradient*** problem which broadly appears in recurrent models. This problem is similar to the gradient propagation issue in training deep networks without residual connections, but occurs along the sequence dimension. Here we derive it with a simplified formulation $\boldsymbol{y}_t = \boldsymbol{F}(\boldsymbol{y}_{t-1}; \theta)$ where $\boldsymbol{y}$ is output and θ denotes the parameters of the SSM $\boldsymbol{F}$. We have

$$
\begin{aligned}
d\boldsymbol{y}_t &= \nabla_\theta \boldsymbol{F}(\boldsymbol{y}_{t-1})d\theta + \nabla_{\boldsymbol{y}}\boldsymbol{F}(\boldsymbol{y}_{t-1})d\boldsymbol{y}_{t-1} \\
&= \nabla_\theta \boldsymbol{F}(\boldsymbol{y}_{t-1})d\theta + \nabla_{\boldsymbol{y}}\boldsymbol{F}(\boldsymbol{y}_{t-1})(\nabla_\theta \boldsymbol{F}(\boldsymbol{y}_{t-2})d\theta \\
&+ \nabla_{\boldsymbol{y}}\boldsymbol{F}(\boldsymbol{y}_{t-2})d\boldsymbol{y}_{t-2}) = \cdots \\
&= (\nabla_\theta \boldsymbol{F}(\boldsymbol{y}_{t-1}) + \nabla_{\boldsymbol{y}}\boldsymbol{F}(\boldsymbol{y}_{t-1})\nabla_\theta \boldsymbol{F}(\boldsymbol{y}_{t-2}) + \cdots)d\theta.
\end{aligned}
$$

Given a loss $L(\boldsymbol{y}_T)$ applied to the T-th token, we have $dL = \nabla_{\boldsymbol{y}}L(\boldsymbol{y}_T)d\boldsymbol{y}_t$ and gradient of parameters $\Delta\theta$ equals

$$
\nabla \boldsymbol{y} L(\boldsymbol{y}_T)(\nabla_\theta \boldsymbol{F}(\boldsymbol{y}_{t-1}) + \nabla_{\boldsymbol{y}}\boldsymbol{F}(\boldsymbol{y}_{t-1})\nabla_\theta \boldsymbol{F}(\boldsymbol{y}_{t-2}) + \cdots),
$$

where repeated multiplications of gradients appear:

$$
\nabla_{\boldsymbol{y}}\boldsymbol{F}(\boldsymbol{y}_{t-1})\nabla_{\boldsymbol{y}}\boldsymbol{F}(\boldsymbol{y}_{t-2})\nabla_{\boldsymbol{y}}\boldsymbol{F}(\boldsymbol{y}_{t-3})\cdots
$$

As derived, the number of repeated gradient multiplications
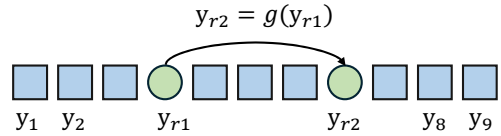
$$y_{r2} = g(y_{r1})$$

depends on the number T. Here we show a simple case of Mamba® with nine image tokens and two registers. As we employ a *reduce-and-concat* module, the two registers are bound together by $\boldsymbol{y}_{r2} = g(\boldsymbol{y}_{r1})$. The gradient propagation from $\boldsymbol{y}_{r2}$ to $\boldsymbol{y}_1$ can be written as

$$
d\boldsymbol{y}_{r2} = \nabla_{\boldsymbol{y}_1}\boldsymbol{F}(\boldsymbol{y}_{r2})d\boldsymbol{y}_1 + \nabla_{\boldsymbol{y}_{r1}}\boldsymbol{F}(\boldsymbol{y}_{r2})\nabla_{\boldsymbol{y}_1}\boldsymbol{F}(\boldsymbol{y}_{r1})d\boldsymbol{y}_1,
$$

where the second term only involves four gradient multiplications. If $\boldsymbol{y}_{r1}$ and $\boldsymbol{y}_{r1}$ are not bound together by g, the number of gradient multiplications becomes eight.